Transient double diffusion in a stably stratified fluid layer heated from below

M. Kazmierczak and D. Poulikakos
Mechanical Engineering Department, University of Illinois at Chicago,
P.O. Box 4348, Chicago, IL, USA

A series of two-dimensional transient numerical simulations is presented for the problem of double diffusion in a horizontal fluid layer linearly stratified in a stable manner with a salt gradient, and heated from below. For the numerical simulations the complete form of the governing equations, subject to the usual Boussinesq approximation, is utilized. A constant heat flux condition is imposed at the bottom warm wall of the system that generates a single well-mixed flow region which grows with time. The growth of the bottom region and the increase of the local and average bottom wall temperature are investigated. Furthermore, results are presented that aim to improve our understanding on the effect of the geometric aspect ratio of the system (H/L) as well as the effect of the ratio of the thermal to the solutal Rayleigh number (stability ratio, $\chi = Ra/Ra_s$) on the evolving temperature, concentration and flow fields. Overall, the trends identified by earlier studies on double diffusion in a horizontal fluid layer are observed and a wealth of new information is reported.

Keywords: double diffusion; transient; numerical simulations

Introduction

Double diffusive convection is a topic of current interest to many researchers in the area of heat transfer and fluid mechanics. The reason for this interest stems from the numerous engineering applications of double diffusive convection. To this end, the necessity for a better understanding of oceanographic phenomena triggered the initiation of fundamental studies in the area of double diffusion about two decades ago.[1–4] Later, numerous studies were motivated by the need to predict and improve the performance of solar ponds[5–7] as solar engineering reached maturity and became a distinct subfield in heat transfer. More recently, attempts are being made to determine the effect of double and multicomponent diffusion in crystal growth, coating, and casting processes.[8,9]

Despite the research efforts of the past, numerous questions pertinent to the phenomenon of double diffusion still remain unanswered. With reference to the problem of interest, namely, a horizontal fluid layer linearly stratified in a stable manner (with the help of a species solution) and heated from below, the theoretical modeling existing up to date needs considerable improvement. For example, for the situation in which the magnitude of the applied bottom heat flux is relatively low, such as in solar ponds, it is observed that a single, warm, well-mixed region forms near the bottom. This region is separated from the overlaying fluid by a boundary layer (Figure 1(a)). Most of the current models (Refs. 10 and 11 and references therein) used for the prediction of the behavior of the above described phenomenon are rather crude and focus on the gross system behavior. To elaborate, all the existing models are one-dimensional, they rely on the input of empirical correlations and constants and they offer little information on the flow structure in the system. Furthermore, even the mechanism responsible for the transfer of energy and species across the boundary layer, essential for continuous growth of the mixed layer, is not well understood and is still under debate.[12]

The purpose of the present study is to present a theoretical (numerical) investigation free from the above shortcomings. The full unsimplified form of the governing equations is used to predict the two-dimensional transient behavior of a mixture of a fluid and a chemical species whose initial density distribution decreases linearly as we move away from the bottom surface, when the layer is subjected to sudden heating at the bottom surface. The developing temperature, flow and concentration fields are determined and several important findings improving our fundamental understanding of the problem are reported.

In a recent study, Ungan and Bergman[13] considered a problem similar to the one in this paper. However, they used "symmetry" and numerically solved "half" of the problem. In stability problems like the present, the use of symmetry is very questionable. The transient evolution of the phenomenon depends on the initial "perturbation" imposed on the system. Unicellular flow or flow with an odd number of cells is possible in the transient region. Imposing symmetry does not allow for the above-mentioned flow structures and the related temperature and concentration fields. Multiple steady-states have also been observed, depending on different initial perturbations of the flow field.[14–17]

Mathematical formulation

The system of interest in the present study is shown schematically in Figure 1(b). Two horizontal solid walls bound from above and from below a mixture of a fluid and a chemical species (such as water and a salt), the density of which decreases linearly as the distance from the bottom wall increases. The two side walls of the system are also solid. Initially, the fluid is isothermal and at rest. Suddenly, a constant heat flux is applied at the bottom wall and starts warming up the system. The remaining

Address reprint requests to Dr. Kazmierczak at the Mechanical Engineering Department, University of Akron, Akron, OH 44325, USA.

Received 24 June 1988; accepted 5 June 1989

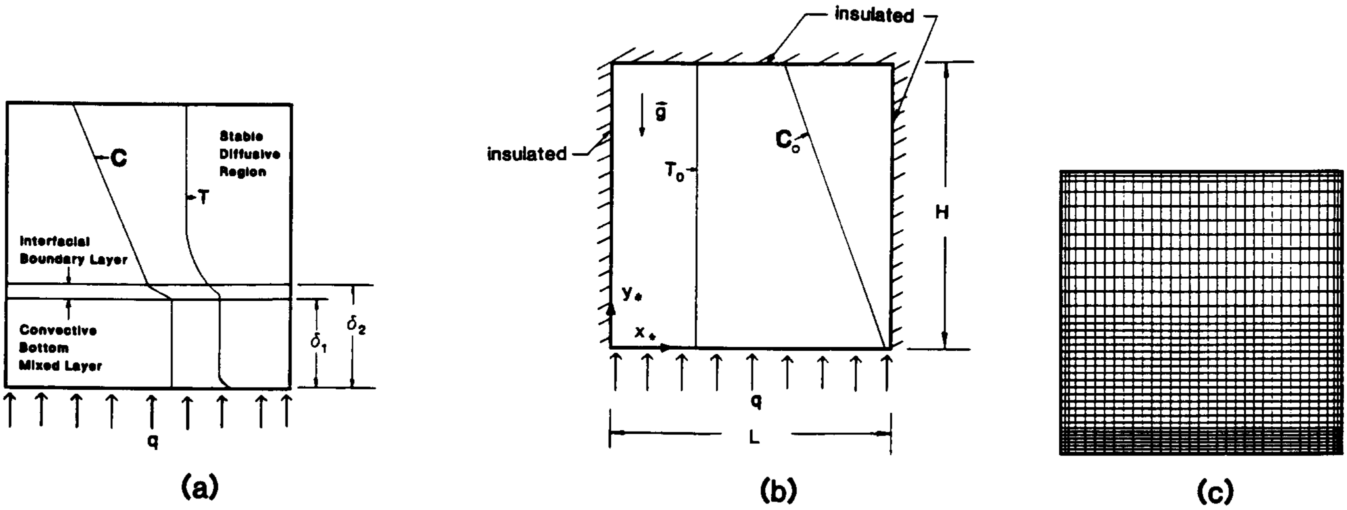

Figure 1 System of interest: (a) one dimensional single mixed layer behavior at large time, (b) initial conditions, (c) computational grid

three walls are assumed insulated. Because of the scenario described above, heat, species, and fluid transport are initiated in the system. The equations governing this transport (continuity, momentum, energy, and species conservation with the Dufour and Soret effects ignored) are

$$\nabla \cdot \mathbf{u}_* = 0 \tag{1}$$

$$\frac{\partial \mathbf{u}_*}{\partial t_*} + \mathbf{u}_* \cdot \nabla \mathbf{u}_* = -\frac{1}{\rho_0} \nabla P_* + \nu \nabla^2 \mathbf{u}_* - \mathbf{g}[1 - \beta(T_* - T_0) + \beta_c(C_* - C_0)] \tag{2}$$

$$\frac{\partial T_*}{\partial t_*} + \mathbf{u}_* \cdot \nabla T_* = \alpha \nabla^2 T_* \tag{3}$$

$$\frac{\partial C_*}{\partial t_*} + \mathbf{u}_* \cdot \nabla C_* = D \nabla^2 C_* \tag{4}$$

In the above equations $\mathbf{u}_*$ is the velocity vector ($\mathbf{u}_* = ui + vj$), P_* the pressure, T_* the temperature, C_* the species concentration, t_* the time, ρ the fluid density, ν the kinematic viscosity, $\mathbf{g}$ the gravitational acceleration vector, and α and D the thermal and mass diffusivities of the solution respectively. Subscript * denotes a dimensional quantity and subscript 0 denotes the initial reference state. In accordance with the usual Boussinesq approximation, the fluid density and thermophysical properties are assumed to be constant everywhere except in the buoyancy force term of the momentum equation (Equation 2) where the density follows the linear state equation

$$\rho = \rho_0[1 - \beta(T_* - T_0) + \beta_c(C_* - C_0)] \tag{5}$$

Quantities β and β_c are the thermal and concentration

Notation

c_p	Specific heat at constant pressure
C	Concentration
D	Mass diffusivity
f	Dummy variable
g	Gravitational acceleration
H	Height of fluid layer
k	Thermal conductivity of the fluid
L	Horizontal length of the fluid layer
Le	Lewis number, α/D
m	Number of horizontal grid lines
n	Number of vertical grid lines
P	Pressure
Pr	Prandtl number, ν/α
q	Heat transfer rate per unit area
Ra	Thermal Rayleigh number, $g\beta qH^4/k\alpha\nu$
Ra_s	Solutal Rayleigh number, $g\beta_c\left(\frac{dC_*}{dy_*}\right)_0 H^4/\alpha\nu$
t	Time
T	Temperature
u	Horizontal velocity component
v	Vertical velocity component
x	Horizontal Cartesian coordinate
y	Vertical Cartesian coordinate
α	Thermal diffusivity, $k/\rho c_p$
β	Coefficient of thermal expansion
β_c	Coefficient of concentration expansion
δ_1	Mixed layer height, Figure 1a
δ_2	Boundary layer height, Figure 1a
μ	Viscosity
ν	Kinematic viscosity, μ/ρ
ρ	Fluid density
ω	Vorticity
χ	Ratio of thermal Rayleigh number to the solutal Rayleigh number, $\mathrm{Ra}/\mathrm{Ra}_s$
Ψ	Stream function

Subscripts

i, j	Nodal location
b	Bottom wall
b_0	Bottom wall at initial condition
T	Top wall
T_0	Top wall at initial condition
0	Initial reference condition
*	Dimensional quantity

Superscripts

r	Iteration number
$\bar{}$	Denoting an average quantity over x

expansion coefficients

$$\beta = -\frac{1}{\rho_0}\left(\frac{\partial\rho}{\partial T}\right)_{P,C} \tag{6}$$

$$\beta_c = -\frac{1}{\rho_0}\left(\frac{\partial\rho}{\partial C}\right)_{P,T} \tag{7}$$

As discussed earlier in this section, the boundary conditions of the problem represent the fact that all walls of the system are solid, generate no species, and all are adiabatic except for the bottom wall at which a constant heat flux is applied. With respect to the coordinate system shown in Figure 1(b) these boundary conditions read

$$\begin{aligned} &u_* = v_* = 0, \quad q = -k\frac{\partial T_*}{\partial y_*},\ \frac{\partial C_*}{\partial y_*} = 0; \quad \text{at } y_* = 0 \\ &u_* = v_* = 0, \quad \frac{\partial T_*}{\partial y_*} = \frac{\partial C_*}{\partial y_*} = 0; \quad \text{at } y_* = H \\ &u_* = v_* = 0, \quad \frac{\partial T_*}{\partial x_*} = \frac{\partial C_*}{\partial x_*} = 0; \quad \text{at } x_* = 0, L \end{aligned} \tag{8}$$

The initial conditions necessary to complete the mathematical formulation are

$$t = 0: \quad u_* = v_* = 0, \quad T_* = T_0,\ C_* = \left(\frac{dC_*}{dy_*}\right)_0 y_* + C_{*_{b_0}} \tag{9}$$

everywhere in the system.

Before attempting to solve the system of Equations 1–4 and 8–9 it is convenient to cast these equations in dimensionless form and to write them with respect to the Cartesian system of Figure 1(b). The dimensionless parameters necessary to perform this task are defined as

$$\begin{aligned} &x = x_*/H, \quad y = y_*/H, \quad u = u_*/(\alpha/H), \quad v = v_*/(\alpha/H) \\ &T = (T_* - T_0)/(qH/k), \quad C = \frac{-(C_* - C_{*_{T_0}})}{H\left(\dfrac{dC_*}{dy}\right)_0}, \quad t = t_*/(H^2/\alpha) \end{aligned} \tag{10}$$

In addition, the dimensionless streamfunction Ψ, and vorticity, ω, are introduced

$$u = \frac{\partial\Psi}{\partial y}, \quad v = -\frac{\partial\Psi}{\partial x}, \quad \omega = \nabla^2\Psi \tag{11}$$

Note that by definition, the streamfunction satisfies the continuity equation. Furthermore, the two momentum equations can be combined to eliminate the pressure gradient and create a unique vorticity equation. After the above manipulations, the dimensionless governing equations and boundary and initial conditions read

$$\frac{\partial\omega}{\partial t} + \frac{\partial}{\partial x}(u\omega) + \frac{\partial}{\partial y}(v\omega) = Pr\nabla^2\omega + \mathrm{Ra}Pr\frac{\partial T}{\partial x} + \mathrm{Ra}_s Pr\frac{\partial C}{\partial x} \tag{12}$$

$$\frac{\partial T}{\partial t} + \frac{\partial}{\partial x}(uT) + \frac{\partial}{\partial y}(vT) = \nabla^2 T \tag{13}$$

$$\frac{\partial C}{\partial t} + \frac{\partial}{\partial x}(uC) + \frac{\partial}{\partial y}(vC) = \frac{1}{\mathrm{Le}}\nabla^2 C \tag{14}$$

for $t > 0$

$$\begin{aligned} &\Psi = 0, \quad -1 = \frac{\partial T}{\partial y}, \quad \frac{\partial C}{\partial y} = 0 \quad \text{at } y = 0 \\ &\Psi = 0, \quad \frac{\partial T}{\partial y} = \frac{\partial C}{\partial y} = 0 \quad \text{at } y = 1 \\ &\Psi = 0, \quad \frac{\partial T}{\partial x} = \frac{\partial C}{\partial x} = 0 \quad \text{at } x = 0, 1 \end{aligned} \tag{15}$$

Initially ($t = 0$)

$$\Psi = \omega = 0, \quad T = 0, \quad C = 1 - y, \quad \text{everywhere} \tag{16}$$

The nondimensionalization process yielded the appearance of four dimensionless groups

$$\mathrm{Ra} = \frac{g\beta qH^4}{k\alpha\nu} \tag{17}$$

$$\mathrm{Ra}_s = \frac{g\beta_c\left(\dfrac{dC_*}{dy_*}\right)_0 H^4}{\alpha\nu} \tag{18}$$

$$Pr = \nu/\alpha \tag{19}$$

$$\mathrm{Le} = \alpha/D \tag{20}$$

Ra is the thermal Rayleigh number appropriate for the constant heat flux boundary condition and Ra_s is the solutal Rayleigh number based on the initial concentration gradient. It is worth noting that the thermal Rayleigh number is proportional to the strength of the destabilizing bottom heat flux whereas the solutal Rayleigh number represents the opposing initial stabilizing concentration gradient. The relative influence of the two is often represented by the stability ratio

$$\chi = \mathrm{Ra}/\mathrm{Ra}_s \tag{21}$$

The remaining two dimensionless groups are the Prandtl number and Lewis number, respectively.

Numerical solution

The problem modeled mathematically in the previous section was solved numerically using a finite difference method. The equations were discretized with the help of the control volume formulation.[18] The heat and mass fluxes across the boundaries of each control volume were calculated via the power law scheme.[19] The resulting system of simultaneous algebraic equations was solved by using an iterative point by point method. Relation was necessary to aid convergence of the vorticity equation. A typical value of the underrelaxation parameter was 0.4 for the vorticity equation. No relaxation was needed for the energy and species equations.

Because of the nature of the boundary conditions, no steady-state exists and the transient behavior of the system is sought. The solution progressed as follows: starting from the initial conditions, the vorticity, energy and species equations were solved simultaneously for the first time step. Next, the time was advanced and the solution for the second time step was obtained starting with the converged solution of the first time step. This process was repeated until a desired time after which the calculations were terminated. The time step used for most of the numerical simulations was $\Delta t \approx 10^{-5}$. The following convergence criterion was satisfied at each time step

$$\frac{\sum_{i,j} |f^{r+1}_{i,j} - f^{r}_{i,j}|}{\sum_{i,j} |f^{r+1}_{i,j}|} < \varepsilon \tag{22}$$

where f stands for ω, Ψ, T or C, r is the iteration number, and ε is a prescribed error ($\varepsilon = 10^{-5}$ for the majority of the runs).

The grid size used for the computations was obtained based on a trial and error procedure. After some experimentation with uniform grids it became clear that a nonuniform grid was necessary to yield reasonable computational accuracy within manageable computer time. The nonuniform grid fineness shown in Figure 1(c) was used in most of the runs. For the case of a square layer ($H/L=1$) this grid consists of $m=38$ horizontal grid lines and $n=36$ vertical grid lines. Note that the bottom of the layer is populated rather densely with grid points relative to the top of the layer. This reflects the fact that during the time domain investigated in this study, most of the flow, heat, and species transport occurred in the vicinity of the bottom wall. For the case $H/L=0.5$ the number of the vertical grid lines was doubled. The chosen grid performed very well and resulted in both accuracy and savings in computational time. Increasing the grid fineness caused no discernible changes in the results. It is worth stressing that savings in computational time are important in the present study because the solution of the present problem requires large amounts of computational time, of the order of hours for a typical run on an IBM 3081 computer.

An important issue related to the numerical procedure is that of the initial conditions. As stated clearly by previous investigators of natural convection problems,[14–17] using uniform conditions in the horizontal direction of the type reported in Equation 15 to initiate the solution yields no flow in the system. Flow may ensue after a large time because of artificial nonuniformities caused by truncation errors. In the present double diffusion problem, initiation of the flow by truncation errors requires unrealistically large time because of the additional resistance to flow imposed by the species concentration gradient in the system. Therefore, the system needs to be perturbed (at least at early times), so that a sustainable flow field exists in the system and triggers the convection phenomenon. In natural convection problems (in the absence of the species diffusion in the system) several approaches have been reported in the literature to initiate flow in a horizontal layer heated from below. Ozoe *et al.*,[14] in their study of three-dimensional natural convection in a cube heated from below, used two hot and two cold spots located inside the system to initiate the flow. They found that the location of the spots dictated the orientation of the resulting flow cell. Moya *et al.*,[15] in their study of natural convection in a horizontal fluid-saturated porous layer heated from below and cooled from above, assumed that a flow pattern existed in the system initially. They obtained this initial flow by solving the same problem but at a small angle of inclination. The flow pattern so obtained was used as the initial "guess" for the flow field inside a perfectly horizontal layer. A similar approach was adopted by Vasseur *et al.*[16] Vasseur *et al.*[17] used a single flow cell, obtained via the assumption that a parallel flow structure exists in the core region, to trigger flow inside a horizontal layer heated from below and cooled from above with constant heat fluxes. In the present study we followed a procedure involving slight tilting at the system, similar but yet different to what was discussed above. At time $t=0$ the layer was slightly tilted from its perfectly horizontal position by one half of one degree for the numerical runs with aspect ratio $H/L=1/2$ and by one degree for the numerical runs of aspect ratio $H/L=1$. At very early times, after a sustainable flow was initiated near the bottom wall, the tilt angle was set equal to zero and the enclosure was returned to its perfectly horizontal position for the remainder of the numerical simulation. The above method yields realistic flow, temperature, and concentration fields and has minimum impact on the subsequent development of the phenomenon. In addition, it is easily duplicable both numerically and experimentally.

Extensive tests on the accuracy of the numerical code are reported in Ref. 20 and, for brevity, are not repeated here. To exemplify, however, the present numerical code was used to solve the problem of transient natural convection in a square enclosure with one vertical wall hot and the other cold. The two horizontal walls are adiabatic. The results were compared to those of Patterson and Imberger.[21] The streamline and isotherm patterns obtained with our code were practically identical to those of Patterson and Imberger.[21] For comparable grids, our code also predicted the Nusselt number reported by Patterson and Imberger[21] within 0.2%.

Results and discussion

The numerical simulations were carried out in a systematic way such that the effect of the major parameters of the transient double diffusion phenomenon is documented. These parameters are the stability ratio, χ and the geometric aspect ratio of the layer, H/L. Because of the large amounts of computational time each numerical simulation required, care was exercised to obtain only the necessary number of numerical simulations that illustrate the physics of the problem. The additional two parameters of the problem, namely, the Prandtl number and the Lewis number, were held fixed throughout this study.

$$Pr=7, \qquad \mathrm{Le}=100 \tag{23}$$

These values are representative of water–salt mixtures. A summary of all the numerical simulations is shown in Table 1. Note that the values of Ra and Ra_s used in this study are representative of laboratory experiments. However, the numerical simulations last long enough for our results to be representative of double diffusion in solar ponds. Taking into account the fact that the numerical simulations are terminated at $t=0.015$, one can easily estimate through Equation 10 that, for a layer of height $H=1\text{m}$ or the corresponding, dimensional time is $t_* \sim 30\,\text{hr}$ which, in an order of magnitude sense, corresponds to time scales observed in solar ponds.

Figures 2–4 report results for the flow, temperature, and species concentration fields for $\chi=3$ ($\mathrm{Ra}=3\times10^9$, $\mathrm{Ra}_s=10^9$) and $H/L=0.5$ (Table 1). In this case, flow first appeared at $t\approx10^{-3}$ and by $t\approx1.5\times10^{-3}$ there is enough flow to cover the entire bottom surface. At this time, the initial perturbation to the system was removed (the one half of one degree tilt angle was set equal to zero and the system was repositioned to its perfectly horizontal position).

Figures 2(a), 3(a), and 4(a) show the predicted flow, temperature, and concentration fields at $t=1.75\times10^{-3}$ when a well-mixed bottom region becomes clearly evident. The flow field (Figure 2(a)) consists of a row of cells located at the very bottom with adjacent cells flowing in opposite directions. No discernible flow occurs above, in the "stable diffusive region" where the heating effect of the bottom wall is hardly felt (Figure 3(a)). From the concentration field (Figure 4(a)) it is obvious that the flow has caused thorough mixing of the solution at the bottom whereas the concentration gradient above remains unchanged. As time progresses, the mixed layer height increases. The predicted contours at $t=4.25\times10^{-3}$ are shown in Figures 2(b), 3(b), and 4(b). Note that the number of cells decreases as

Table 1 Summary of numerical simulations

Ra	Ra_s	X	Pr	Le	H/L	Grid (m × n)
3×10^9	1×10^9	3	7	100	0.5	37 × 65
3×10^9	1×10^9	3	7	100	1	37 × 35
3×10^9	3×10^8	10	7	100	1	37 × 35
3×10^8	1×10^8	3	7	100	1	37 × 35

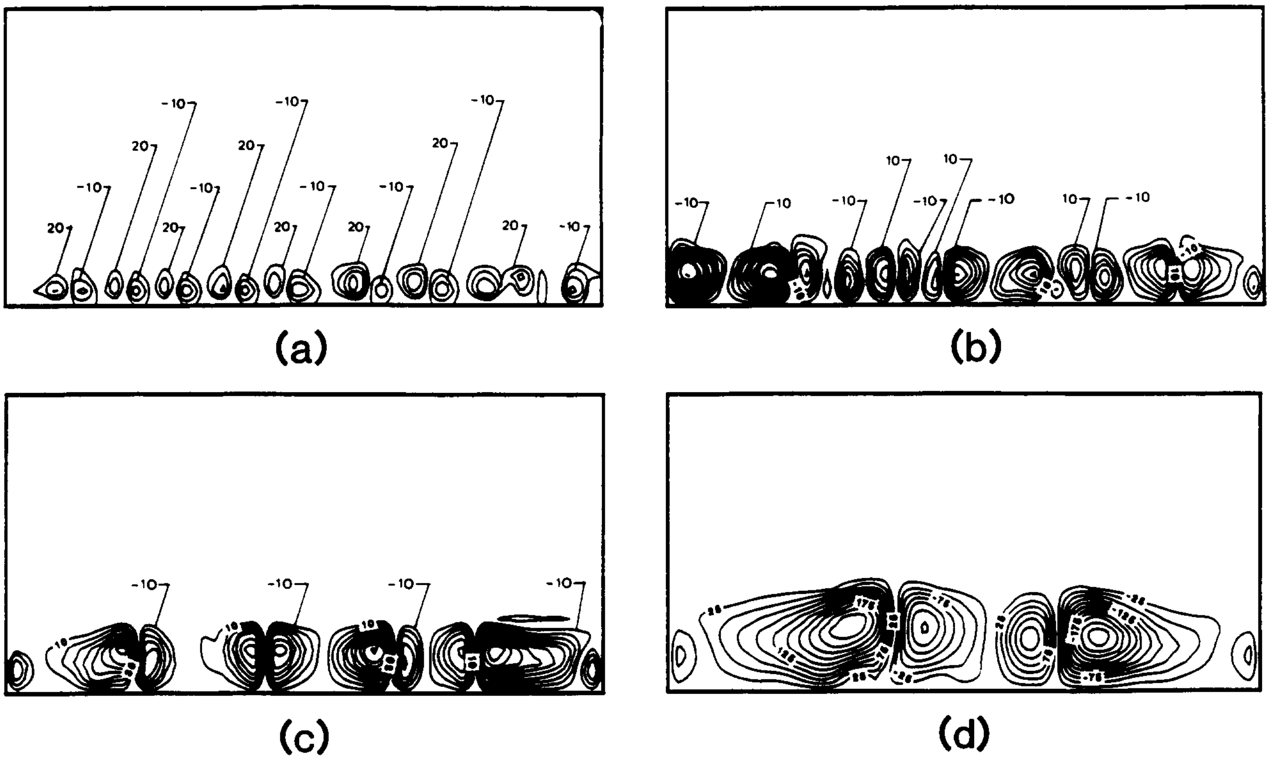

Figure 2 Streamlines for Ra$=3\times10^9$, Ra$_s=10^9$, $\chi=3$, $H/L=0.5$ at characteristic times. Contours are spaced equidistantly: (a) $t=0.00175$, (b) $t=0.00425$, (c) $t=0.00550$, (d) $t=0.01200$

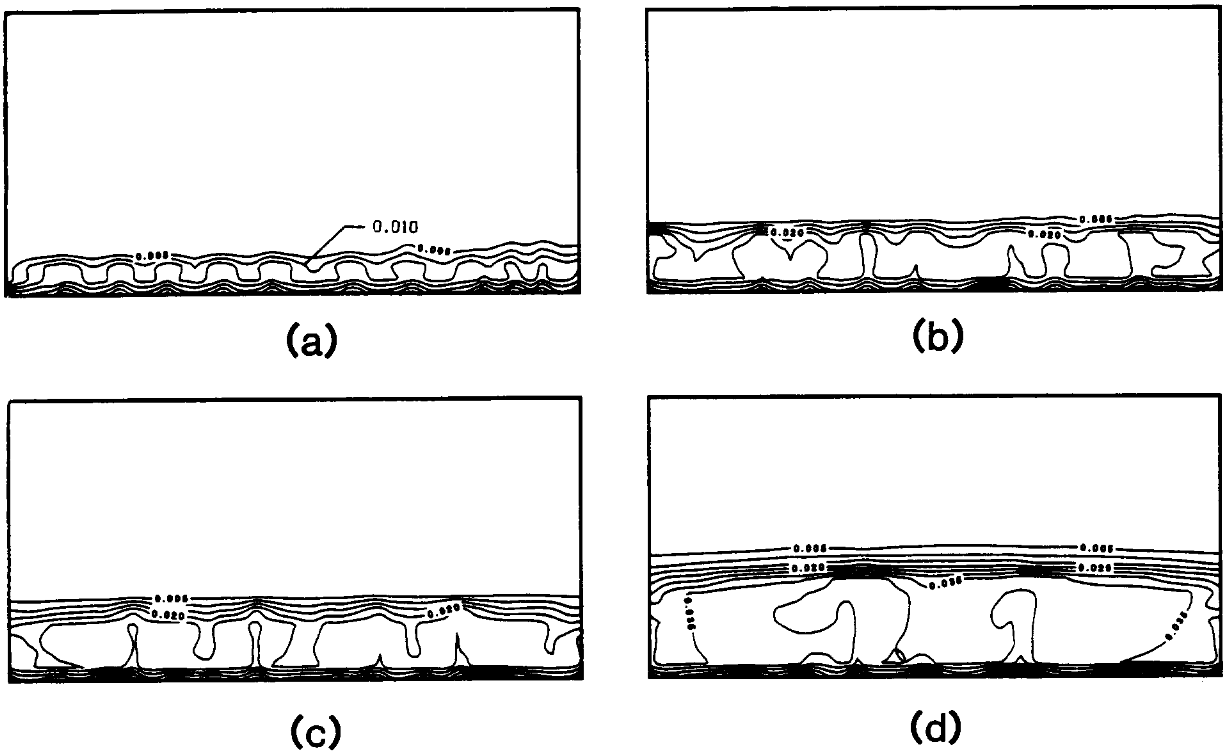

Figure 3 Isotherms for Ra$=3\times10^9$, Ra$_s=10^9$, $\chi=3$, $H/L=0.5$ at characteristic times. Contours are spaced equidistantly: (a) $t=0.00175$, (b) $t=0.00425$, (c) $t=0.00550$, (d) $t=0.01200$

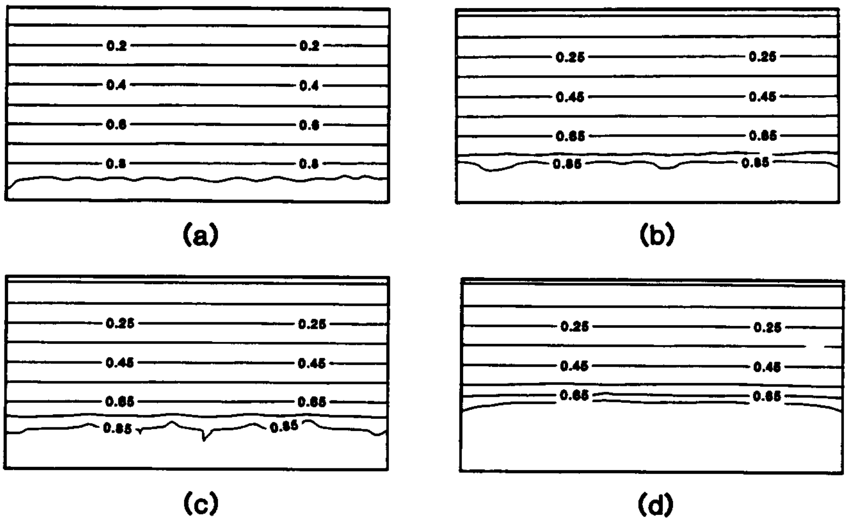

Figure 4 Equal concentration lines for Ra = 3×10^9, $Ra_s=10^9$, $\chi=3$, $H/L=0.5$ at characteristic times. Contours are spaced equidistantly: (a) $t=0.00175$, (b) $t=0.00425$, (c) $t=0.00550$, (d) $t=0.0120$

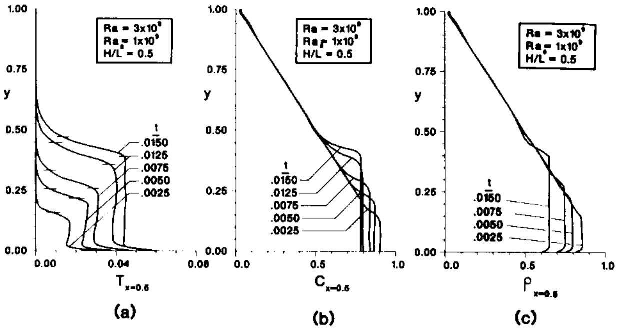

Figure 5 Centerline profiles for $Ra=3\times10^9$, $Ra_s=10^9$, $\chi=3$, $H/L=0.5$: (a) temperature, (b) concentration, (c) density

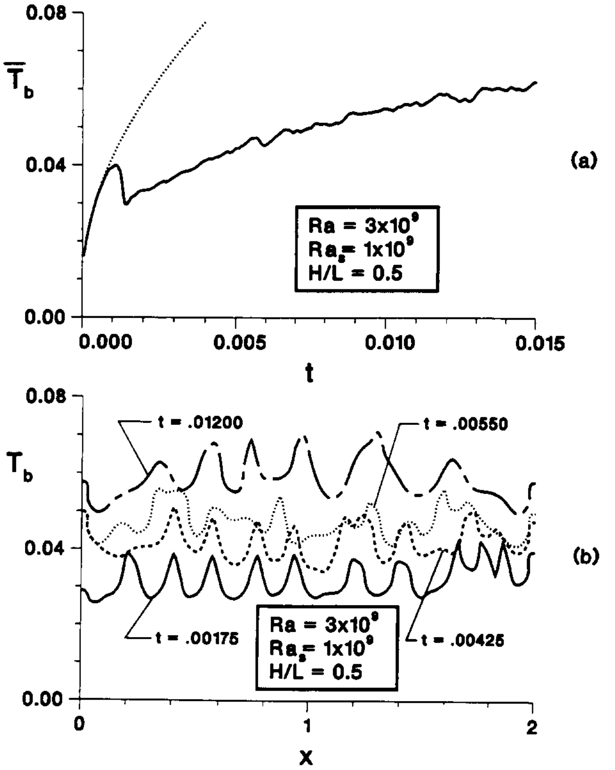

Figure 6 Bottom wall temperature for $Ra=3\times10^9$, $Ra_s=10^9$, $\chi=3$, $H/L=0.5$: (a) dependence of average temperature on time, (b) dependence on horizontal position

the mixed layer height increases. Small cells have merged to form larger cells of stronger intensity. The pattern of cell number reduction continues (Figures 2(c)–2(d)) until at $t=1.2\times10^{-2}$ only four major cells remain. Although the flow pattern is strongly two-dimensional, note that the resulting temperature and concentration fields depend mainly on the vertical direction.

Figures 5(a), 5(b), and 5(c) show the centerline temperature, concentration, and density profiles at various times. Comparable profiles were predicted at other horizontal locations. All temperature profiles feature a uniform temperature in the mixed layer (except at the very bottom where a thin thermal boundary layer exists according to the constant heat flux boundary condition) and exhibit a pure conduction-like behavior in the region above. Another interesting observation from comparing the temperature profiles at various times between $t=2.5\times10^{-3}$ and $t=1.5\times10^{-2}$ is that the *thermal* "boundary layer" front between the bottom and the top isothermal regions thickens with time. The species concentration profiles in Figure 5(b) exhibit a behavior similar to the temperature profiles. The bottom well-mixed region is at a uniform concentration. While this region grows, its concentration decreases. The small horizontal lines in Figure 5(a) define the extent of the concentration boundary layer on top of the well-mixed region. It appears that the temperature variation inside the concentration boundary layer is approximately linear. Above the concentration boundary layer the temperature decays exponentially. In addition, Figure 5(a) shows that the temperature gradient inside the concentration boundary layer does not vary appreciably with time.

It is important to note that, for the most part, the density profiles of Figure 5(c) support the claim by Turner[2] that the density steps due to temperature and concentration at the top of the mixed layer are equal and of opposite sign. At the end of the numerical simulation ($t=0.015$), however, a stable density boundary layer appears to develop at the top of the mixed region providing the equivalent of a net stable density step.[2]

The transient response of the bottom wall temperature is shown in Figure 6(a). The mean bottom wall temperature increases rapidly at first, exactly as predicted by the pure conduction solution shown by the dotted line, until at $t\approx10^{-3}$ when convective flow starts which quenches the bottom surface with cooler overlaying fluid entrained from above. After $t\approx$

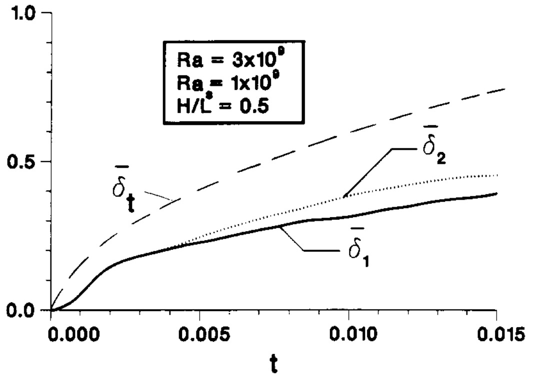

Figure 7 Growth of mixed layer average height ($\bar{\delta}_1$) and interfacial boundary layer average thickness ($\bar{\delta}_2-\bar{\delta}_1$) for $\mathrm{Ra}=3\times10^9$, $\mathrm{Ra}_s=10^9$, $\chi=3$, $H/L=0.5$. Also shown is the distance of the edge of the thermal boundary layer from the bottom wall ($\bar{\delta}_t$)

1.5×10^{-3} when flow is fully established over the entire bottom surface, the bottom mean temperature rises again, but this time at a much slower rate since energy is being transported away from the bottom wall to the well-mixed fluid region above it. The fluctuating nature of the bottom wall temperature is a direct result of the ever-changing flow structure in the system. Figure 6(b) shows the variation of the bottom wall local temperature reported at various times. The maxima in the temperature variation are found to occur in the regions located in between adjacent cells where the flow direction is upwards (away from the wall). Similarly, colder fluid from above travelling downward (toward the bottom wall) is responsible for the appearance of the minima in the temperature distribution.

The growth of the well-mixed bottom layer and the thickness of the interfacial boundary layer separating the bottom well-mixed region and the top stagnant region of the system is illustrated in Figure 7. The solid line represents the top of the well-mixed region (and the bottom of the interfacial boundary layer). The dotted line represents the top of the interfacial boundary layer. The distance between the two lines is the boundary layer thickness. The solid line was calculated by checking the concentration of the bottom layer starting from the bottom wall and moving upward. The top of the well-mixed region was defined as the height at which the species concentration decreases by 2% relative to its value in the well-mixed region. The dotted line was determined by using the same criterion starting from the top and determining the point at which the concentration deviates by 2% relative to its initial value. This procedure was repeated at all χ locations. The values used to construct the lines shown in Figure 7 were obtained after averaging the results at each χ location. It is worth noting that the dependence of the mixed layer height and the boundary layer region on the horizontal position is very weak. Clearly, the concentration boundary layer thickens as time increases. At early times, such a region practically does not exist. It becomes visible after $t\approx5\times10^{-3}$. Before this time, the bottom uniform concentration region and the top linearly stratified region are separated by a sharp interface. As time proceeds and the interfacial boundary layer thickens it is important to note that the stabilizing concentration difference across this region becomes larger. This fact limits the mixed layer growth rate.

Also shown with a dashed line in Figure 7 is the distance of the edge of the thermal boundary layer from the bottom wall. The thermal boundary layer thickens monotonically and advances ahead of the concentration boundary layer. It appears, therefore, that a region exists on top of the concentration boundary layer and inside the thermal boundary layer in which the concentration distribution is linear (the initial concentration distribution) while the temperature decreases exponentially (see also Figure 5(a)). This region thickens as the transient phenomenon progresses.

Having explored in detail the system behavior for a given fixed set of parameters, we now shift our attention to study the effect of these parameters on the double diffusion phenomenon. The first system parameter investigated is the system geometric aspect ratio, $H/L=1$. Referring to Table 1, we see that all the parameters for the second simulation performed have the same values with the parameters in the first simulation except for the aspect ratio which was doubled from $H/L=0.5$ to $H/L=1$. Figures 8–10 report a sequence of flow, temperature, and species concentration fields respectively. Except for the fact that the flow structure contains fewer number of cells, the square system ($H/L=1$) behaves much the same as the longer rectangular system ($H/L=0.5$). The temperature (Figure 9) and the concentration (Figure 10) fields reveal that a single well-mixed layer develops at the bottom wall and grows with time. It was found that the resulting concentration and temperature fields for the square system are the same with those predicted for the longer system. The actual comparison is not shown here for brevity. Based on the above fact, it is concluded that, for systems with $H/L<1$, the effect of aspect ratio on the double diffusion phenomenon is not important. The overall features of these systems are similar to those of infinitely long layers. In all subsequent simulations, the system aspect ratio was set equal to unity to minimize the required computational time.

The second major system parameter investigated is the stability ratio, $\chi=\mathrm{Ra}/\mathrm{Ra}_s$. To determine the effect of increasing χ the third simulation listed in Table 1 was performed. The value of χ was increased from $\chi=3$ to $\chi=10$ by decreasing the solutal Rayleigh number from $\mathrm{Ra}_s=1\times10^9$ to $\mathrm{Ra}_s=3\times10^8$

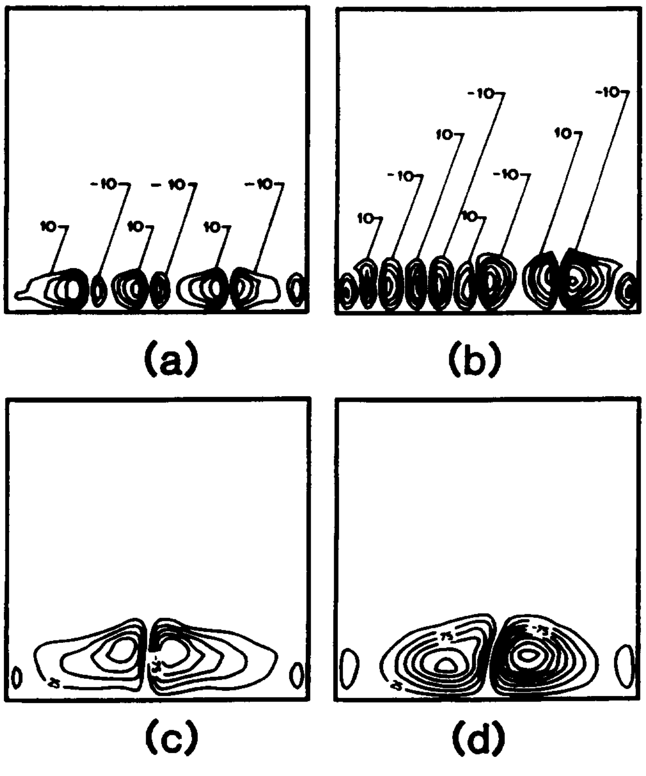

Figure 8 Streamlines for $\mathrm{Ra}=3\times10^9$, $\mathrm{Ra}_s=10^9$, $\chi=3$, $H/L=1$ at characteristic times. Contours are spaced equidistantly: (a) $t=0.0020$, (b) $t=0.0040$, (c) $t=0.0065$, (d) $t=0.0080$

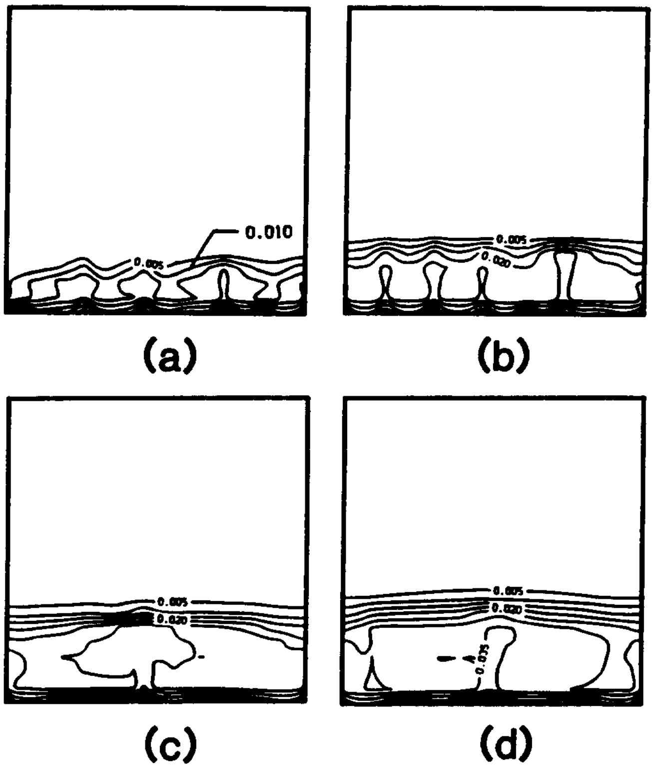

Figure 9 Isotherms for $Ra=3\times10^9$, $Ra_s=10^9$, $\chi=3$, $H/L=1$ at characteristic times. Contours are spaced equidistantly: (a) $t=0.0020$, (b) $t=0.0040$, (c) $t=0.0065$, (d) $t=0.0080$

while keeping all other parameters constant. The sequence of flow, temperature, and concentration fields for this case is reported in Figures 11–13. The impact of increasing χ was drastic. Although a single convective layer formed below a stable diffusion region much like in the previous simulations, several differences are apparent. From Figure 11 we see that the flow is much stronger and that the convective region grows much faster. This more vivid flow, results in significant horizontal temperature (Figure 12) and horizontal concentration (Figure 13) gradients in the system. In addition, the interface boundary layer is no longer horizontal. For comparison, the mean bottom wall temperature is plotted in Figure 14(a) for $\chi=3$ and $\chi=10$. Figure 14(b) shows a similar comparison for the mixed layer height. Several differences are immediately evident. Increasing χ increases the rate at which the mixed layer grows (Figure 14(b)). This fact is reflected in the mean bottom temperature (Figure 14(a)) that departs from the pure conductive solution sooner and is maintained at a lower value. Note also that the mean mixed layer height is no longer smooth but it fluctuates with time, a direct consequence of the flow field discussed earlier.

Next, the effect of decreasing both the thermal Rayleigh number (Ra) and the solutal Rayleigh number (Ra_s) while keeping the stability ratio, the same ($\chi=3$) is examined. The mean bottom temperature and the mean mixed layer height for the last case in Table 1 ($\chi=3$, $Ra=3\times10^8$, $Ra_s=10^8$), is also plotted in Figures 14(a) and (b), respectively (solid-dash lines). Comparing the two lines for $\chi=3$ in Figure 14(b) we observe that the mixed layer height for the simulation with the lower values of Ra and Ra_s grows slightly slower and the mixed layer is initiated considerably later. This results in a warmer mean bottom temperature (Figure 14(a)).

The flow field development (after the flow initiation stage) is qualitatively the same for the two runs with $\chi=3$ in terms of cell shape, size, and merging characteristics but the magnitude of the flow strength is significantly less for the simulation with the lower Rayleigh numbers. Figure 15 shows the flow, temperature, and concentration fields for the last case in Table 1 at $t=0.01250$. Note that the maximum stream function at $t=0.01250$ is $\Psi_{max}\approx55$ whereas the maximum streamfunction in Figure 8 at the same time was $\Psi_{max}\approx200$. It is then possible to slow down the flow by keeping χ constant and decreasing Ra_s and Ra simultaneously.

Before closing this section, it is necessary to put our numerical results into proper perspective with respect to the experimental findings of Turner[2] and Hupert and Linden.[4] The present numerical simulations did not produce multiple mixed layer growth like some of the experiments by Turner[2] and by Huppert and Linden.[4] It is known that a single well-mixed region exists in double diffusion if the magnitude of the bottom wall heat flux (Ra) is not very high compared to the stabilizing salt gradient (Ra_s), i.e., the stability ratio $\chi=Ra/Ra_s$ is not very large.[11,13] In our numerical simulation, the stability ratio was in the range $3<\chi<10$. In the experiments of Turner[2] and Huppert and Linden,[4] the stability ratios were $\chi=26$ and $\chi=17$ respectively, thus explaining why they observed multiple layer formation and we did not. In this respect, both our numerical results and the experiments of Turner[2] and Huppert and Linden[4] make sense physically. We chose lower values of χ deliberately. Since the present paper is one of few existing 2-D numerical simulations, it focuses on the more manageable single cell formation and aims at improving our fundamental knowledge on its development and growth. Based on the difference stated above, no direct quantitative comparisons between our results and those of Turner[2] and Huppert and Linden[4] are possible.

A second major difference between our work and that of

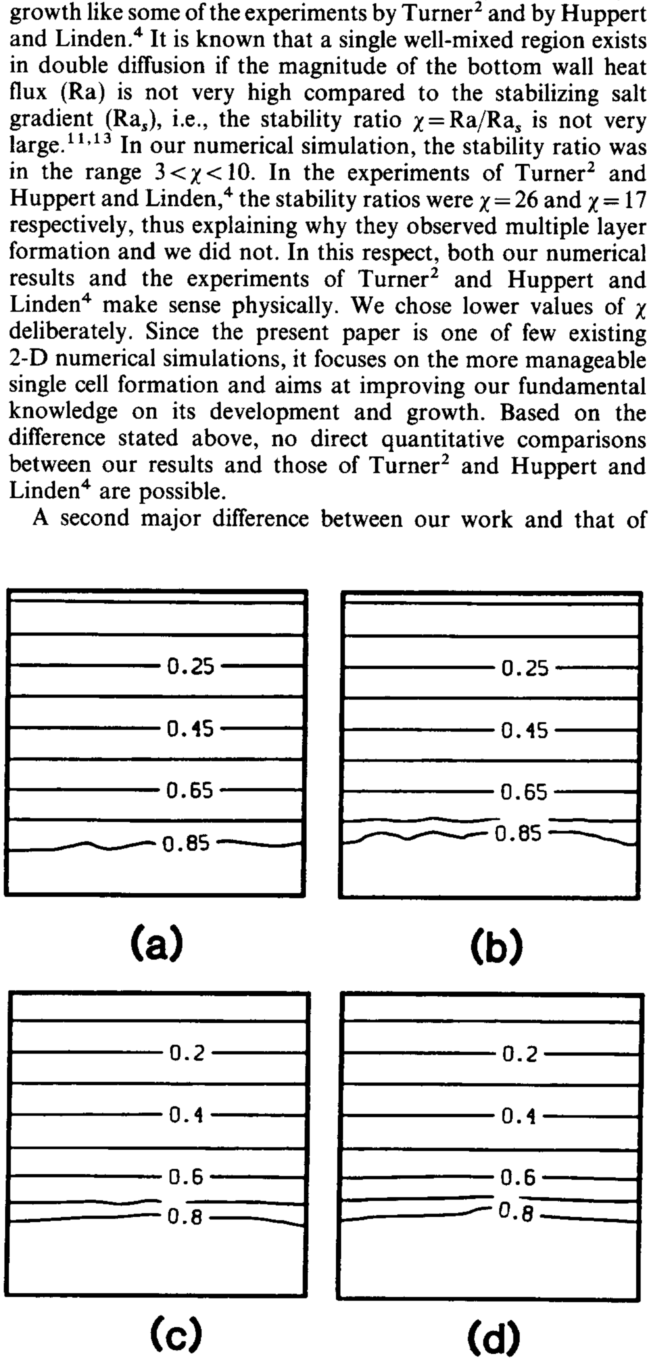

Figure 10 Equal concentration lines for $Ra=3\times10^9$, $Ra=10^9$, $\chi=3$, $H/L=1$ at characteristic times. Contours are spaced equidistantly: (a) $t=0.0020$, (b) $t=0.0040$, (c) $t=0.0065$, (d) $t=0.0080$

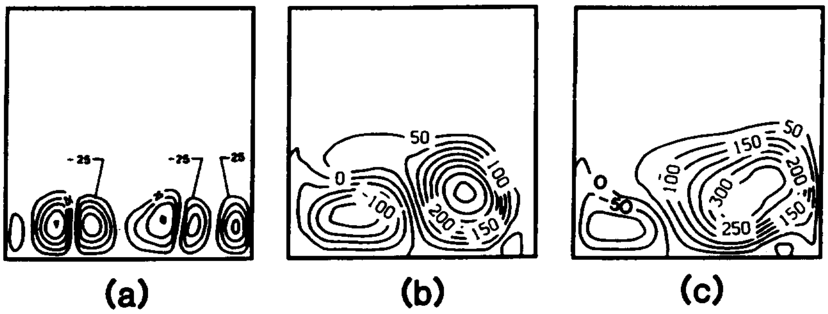

Figure 11 Streamlines for Ra$=3\times10^9$, Ra$_s=3\times10^8$, $\chi=10$, $H/L=1$ at characteristic times. Contours are spaced equidistantly: (a) $t=0.0020$, (b) $t=0.00850$, (c) $t=0.00950$

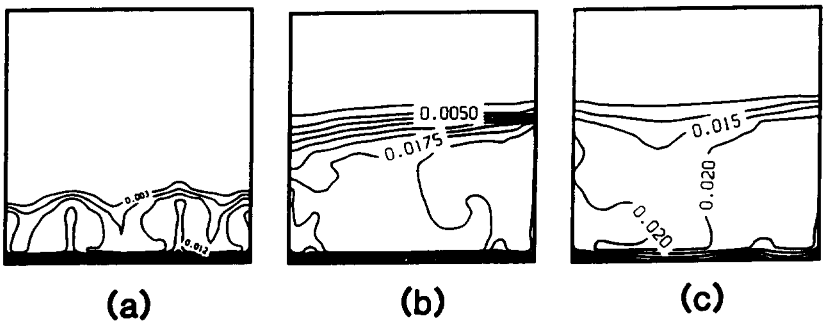

Figure 12 Isotherms for Ra$=3\times10^9$, Ra$_s=3\times10^8$, $\chi=10$, $H/L=1$ at characteristic times. Contours are spaced equidistantly: (a) $t=0.0020$, (b) $t=0.00850$, (c) $t=0.00950$

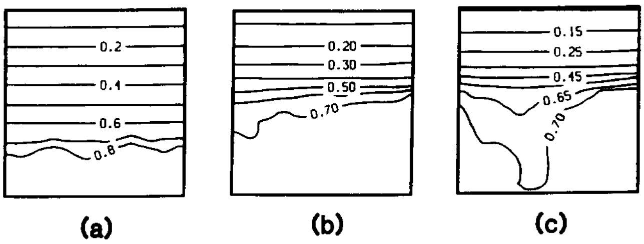

Figure 13 Equal concentration lines for Ra$=3\times10^9$, Ra$_s=3\times10^8$, $\chi=10$, $H/L=1$ at characteristic times. Contours are spaced equidistantly: (a) $t=0.0020$, (b) $t=0.00850$, (c) $t=0.00950$

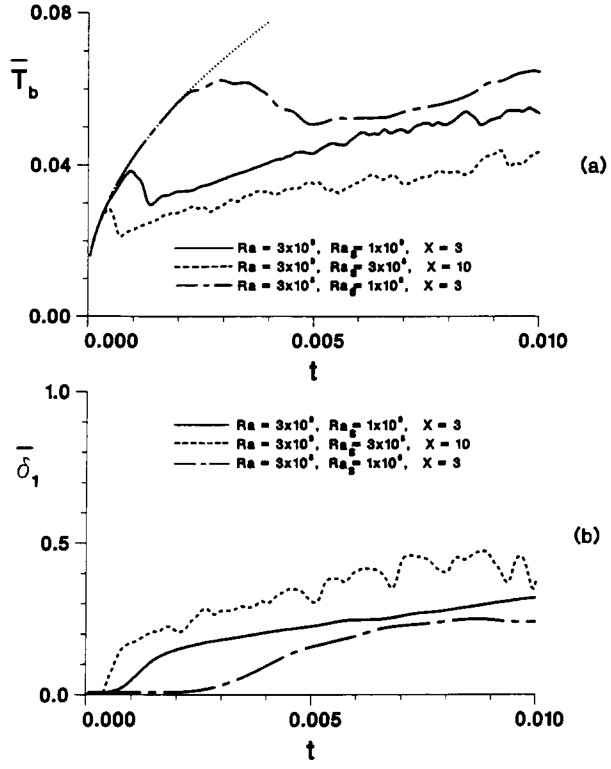

Figure 14 Comparing results from three simulations: (a) average bottom temperature, (b) average bottom layer height

Turner[2] and Huppert and Linden[4] is the magnitude of Ra and Ra$_s$ used in the three studies. The highest Rayleigh numbers in our study were Ra$=3\times10^9$ and Ra$_s=1\times10^9$. In the experiments of Turner, Ra$=3\times10^{11}$ and Ra$_s=1.2\times10^{10}$ was used. In the experiments of Huppert and Linden[4] the corresponding values were Ra$=4\times10^{11}$, Ra$_s=2.4\times10^{10}$. The difference in the thermal Rayleigh numbers between our work and that of Turner[2] or Huppert and Linden[4] is roughly two orders of magnitude. This is why we feel that using a laminar flow model is justifiable in our work, even though Turner[2] observed turbulence and 3-D effects in his experiments. In addition, our values for Ra and Ra$_s$ are based on the total height of the layer. If, in the calculation of Ra and Ra$_s$, the instantaneous height of the "active" well-mixed region is used, the values of the so obtained "instantaneous" Ra and Ra$_s$ will be considerably smaller. For example, at the end of the first simulation the value of the "instantaneous" thermal Rayleigh number was calculated to be Ra$\sim7\times10^8$. For the above reasons as well as for the fact that a laminar flow model is a good first step toward more complex turbulent numerical simulations it is felt that the present laminar numerical simulations are appropriate.

Conclusions

This study presented a numerical investigation of transient two-dimensional double diffusion in a horizontal layer of a liquid solution (such as water and a salt). Initially, the liquid solution was motionless, isothermal, and its density decreased linearly with distance from the bottom wall. The initial density distribution reflects the fact that the species concentration decreased linearly with distance from the bottom wall. At $t=0$ a constant heat flux was applied at the bottom wall.

The results of the investigation provide insight for the

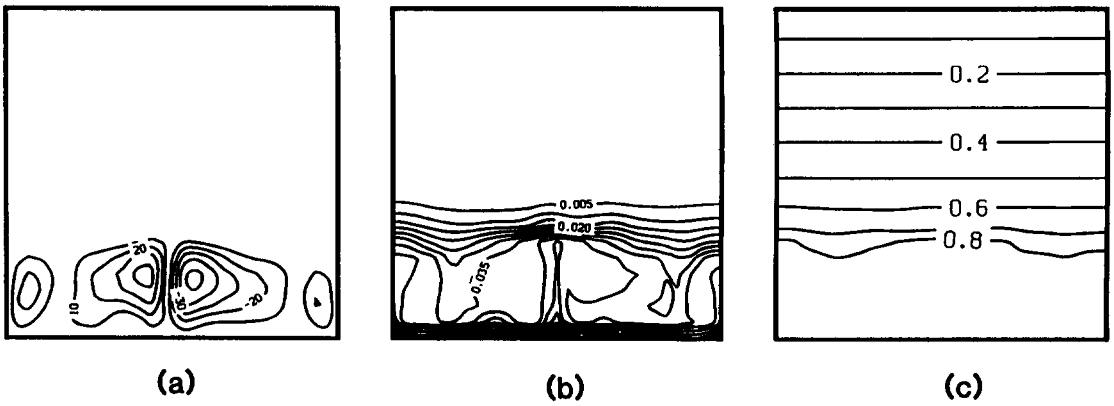

Figure 15 Predicted contours for Ra$=3\times10^8$, Ra$_s=10^8$, $\chi=3$, $H/L=1$ at $t=0.01250$. Contours are spaced equidistantly: (a) streamlines, (b) isotherms, (c) equal concentration lines

growth and the nature of the flow, the temperature and the concentration fields in the system. The flow field is strongly two-dimensional and multicellular. As time progresses the number of cells decreases; pairs of cells merge to create single cells. At early times, all of the flow activity occurs near the bottom wall. The flow region grows with time. The temperature and concentration fields of the flow region are largely one-dimensional, however, increasing the value of the stability parameter, χ, from $\chi=3$ to $\chi=10$ initiates significant two-dimensional effects on the temperature and the concentration fields. This finding has direct implications regarding the range of validity of simple one-dimensional models for double diffusion in horizontal layers. The geometric aspect ratio of the system had very little impact on the phenomenon of interest for the parametric domain examined in this study.

Acknowledgment

Support for this work was provided by NSF through grant ENG 8451144 is appreciated.

References

1 Turner, J. S. The coupled turbulent transports of salt and heat across a sharp density interface. *Int. J. Heat and Mass Transfer*, 1965, **8**, 759–767
2 Turner, J. S. The behavior of a stable salinity gradient heated from below. *J. Fluid Mechanics*, 1968, **33**, 183–200
3 Turner, J. S. *Buoyancy Effects in Fluids*. Cambridge University Press, Cambridge, 1979
4 Huppert, E. and Linden, P. F. On heating a stable salinity gradient from below. *J. Fluid Mechanics*, 1979, **95**, 431–464
5 Rabi, A. and Nielsen, C. E. Solar ponds for space heating. *Solar Energy*, 1975, **17**, 1–12
6 Styris, D. L. and Harling, O. K. The nonconvecting solar pond applied to building and process heating. *Solar Energy*, 1976, **18**, 245–251
7 Tabor, H. Solar ponds. *Solar Energy*, 1981, **27**, 181–194
8 Chen, C. F. and Turner, J. S. Crystallization in a double-diffusive system. *J. Geophys. Res.*, 1980, **85**, 2573–2593
9 Ostrach, S. Fluid mechanics of crystal growth—The 1982 Freeman Scholar Lecture. *Trans. Am. Soc. Mech. Engrs, Series I, J. Fluids Engng.*, 1983, **105**, 5–20
10 Meyer, K. A. A numerical model to describe the layer behavior in salt-gradient solar ponds. *ASME J. Solar Energy Engng.*, 1983, **25**, 63–75
11 Bergman, T. L., Incropera, F. P., and Viskanta, R. A differential model for salt-stratified, double-diffusive systems heated from below. *Int. J. Heat and Mass Transfer*, 1985, **28**, 779–788
12 Incropera, F. P. Buoyancy effects in double-diffusive and mixed convection flows. *Proceedings of the 8th Int. Heat Transfer Conf.*, 1986, **1**, 121–130
13 Ungan, A. and Bergman, T. L. A two-dimensional numerical simulation of a linear stratified thermohaline system heated from below. *Paper No. 87-WA/HT-19*, ASME Winter Annual Meeting, Boston, MA, 1987
14 Ozoe, H., Yamamoto, K., Churchill, S. W., and Sayama, H. Three-dimensional, numerical analysis of laminar natural convection in a confined fluid heated from below. *ASME Paper 76-HT-RR*, 1976
15 Moya, S. L., Ramos, E., and Sen, M. Numerical study of natural convection in a tilted rectangular porous material. *Int. J. Heat and Mass Transfer*, 1987, **30**, 741–756
16 Vasseur, P., Satish, M. G., and Robillard, L. Natural convection in a thin inclined porous layer exposed to a constant heat flux. *Int. J. Heat and Mass Transfer*, 1987, **30**, 537–549
17 Vasseur, P., Robillard, L., and Sen, M. Unicellular convective motion in an inclined fluid layer with uniform heat flux. *Bifurcation Phenomena in Thermal Processes and Convection*, ASME Publication HTD, 1987, **94**, 23–29
18 Roache, P. J. *Computational Fluid Dynamics*. Hermosa, Albuquerque, 1976
19 Patankar, S. V. *Numerical Heat Transfer and Fluid Flow*. McGraw-Hill, New York, 1980
20 Kazmierczak, M. J. Transient double diffusion in a fluid layer and a composite (porous/fluid) layer heated from below. Ph.D. Thesis, University of Illinois at Chicago, Chicago, 1988
21 Patterson, J. and Imberger, J. Unsteady natural convection in a rectangular cavity. *J. Fluid Mechanics*, 1980, **100**, 65–86